

Slowing down Josephson vortex lattice in $\text{Bi}_2\text{Sr}_2\text{CaCu}_2\text{O}_{8+x}$ with pancake vortices

A. E. Koshelev

Materials Science Division, Argonne National Laboratory, Argonne, Illinois 60439

Yu. I. Latyshev

Institute of Radio-Engineering and Electronics, Russian Academy of Sciences, Mokhovaya 11-7, 101999 Moscow, Russia

M. Kunczykowski

Laboratoire des Solides Irradies, CNRS UMR 7642, Ecole Polytechnique, 91128 Palaiseau, France

(dated: January 16, 2022)

We study theoretically and experimentally the influence of pancake vortices on the motion of the Josephson vortex lattice in layered high-temperature superconductors. Mobility of the Josephson vortices in layered superconductors is strongly suppressed by the small amount of pancake-vortex stacks. Moving Josephson vortex lattice forces oscillating zigzag deformation of the pancake-vortex stacks contributing to damping. The salient feature of this contribution is its nonmonotonic dependence on the lattice velocity and the corresponding voltage. Maximum pancake effect is realized when the Josephson frequency matches the relaxation frequency of the stacks. The pancake-vortex damping is strongly suppressed by thermal fluctuations of the pancake vortices. This theoretical picture was qualitatively confirmed by experiments on two mesas prepared out of $\text{Bi}_2\text{Sr}_2\text{CaCu}_2\text{O}_{8+x}$ whiskers. We found that the Josephson-vortex flow voltage is very sensitive to small c-axis magnetic field. The pancake-vortex contribution to the current indeed nonmonotonically depends on voltage and decreases with increasing temperature and in-plane magnetic field. We also found that irradiation with heavy ions has no noticeable direct influence on the motion of the Josephson vortices but dramatically reduces the pancake-vortex contribution to the damping of the Josephson vortex lattice at low temperatures.

I. INTRODUCTION

The layered crystalline structure of the cuprate high-temperature superconductors leads to existence of two types of vortices in these materials, pancake-vortex (PV) stacks¹ induced by the magnetic field component perpendicular to the layers and Josephson vortices (JVs)² created by the magnetic field component parallel to the layers. Repulsive interaction between the vortices of each type results in formation of regular vortex lattices. In particular, the magnetic field applied along the layers generates triangular lattice of the JVs stretched along the layer direction. The anisotropy factor sets the important field scale, $B_{cr} = \phi_0/(2s^2)$, where s is the interlayer periodicity. When the magnetic field exceeds B_{cr} the Josephson vortices homogeneously fill all layers forming a dense lattice². In highly anisotropic materials, like $\text{Bi}_2\text{Sr}_2\text{CaCu}_2\text{O}_{8+x}$ (BSCCO) this field scale is rather moderate ~ 0.5 tesla.

In BSCCO, due to a very weak Josephson interlayer coupling, two types of vortices can coexist in the tilted magnetic field³. The static attractive interaction between JVs and PV stacks⁴ leads to many exotic vortex states, such as mixed chain-lattice state^{5,6,7} and pancake-chains state⁸, and has been used for visualization of JV stacks^{6,9,10}, see recent review¹¹.

Dynamic properties of the crossing-lattices state have been studied in much less details. A particularly interesting topic is dynamic behavior of the JV lattice. An external transport current flowing across the layers drives the JV lattice along the layers. Due to relatively weak

intrinsic dissipation, the Josephson vortices can be accelerated up to very high velocities. Dynamics of the JV lattice in BSCCO have been extensively studied by several experimental groups (see, e.g., Refs. 12,13,14). When magnetic field is tilted at small angle with respect to the layers, the c-axis field component generates small concentration of PV stacks. Alternating in-plane supercurrents of static JV lattice force zigzag deformations of the PV stacks¹⁵, see Fig. 1. It is well known that mobility of JVs is strongly suppressed by a very small amount of PV stacks^{16,17,18}. As a consequence, studying the JV lattice transport always requires a very accurate alignment of the magnetic field with the layers. In spite of that common knowledge, JV lattice dynamics in presence of the PV stacks has never been investigated systematically.

In the case of strong anisotropy, the JV lattice can move through static PV stacks. Even in this case the PV stacks will strongly impede motion of the JV lattice. Dynamic behavior of the PV stack naturally follows from its static configuration. The moving JV lattice forces oscillations of the PV stacks leading to additional dissipation and slowing down the lattice. In this paper we investigate this effect quantitatively in the case of dense JV lattice. Influence of the PV stacks on motion of an isolated JV has been considered theoretically in Ref. 19.

The paper is organized as follows. In Sec. II we present theoretical models describing influence of the PV stacks on motion of the dense JV lattice. We compute the dynamic friction force generated by PV stacks and study suppression of this force by PV fluctuations. We also consider influence of the PV fluctuations on the regular

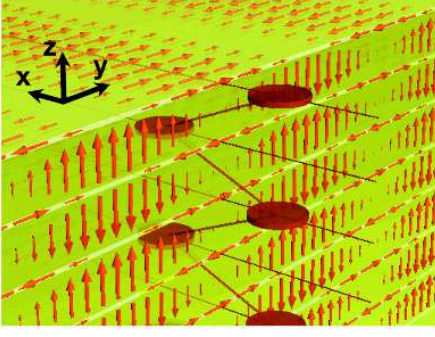


FIG. 1: Sketch of a pancake-vortex stack in presence of the dense JV lattice. The arrows illustrate current distribution of the JV lattice and the discs illustrate pancake vortices. The JV lattice induces zigzag deformation of the stack. Moving lattice induces oscillating zigzag deformations which contribute to dissipation, see animation.

JV flux-flow resistivity and influence of columnar defects on the PV-induced damping of the JV lattice. In Sec. III we present experimental results. Studying the flux-flow of the JV lattice for small c-axis magnetic fields, we extracted the PV contribution to the JV damping and studied its dependence on the voltage, temperature, and in-plane field. We also found that this PV contribution is strongly suppressed by heavy-ion irradiation. In Sec. IV we discuss comparison between the experiment and theory and possible applications of the studied effect.

II. THEORETICAL MODELS

A. Basic model

A general description of JV dynamics in presence of the PV stacks is rather complicated. We consider first the simplest situation, in which influence of the pancake vortices on motion of the JV lattice can be traced in a clearest way. We assume that a strong magnetic field, $B \approx 1$ tesla, is applied in the x - z plane at a very small angle with respect to the layers. Such a magnetic field generates the dense JV lattice and a dilute array of the PV stacks. We neglect both pinning and thermal fluctuations of the pancake vortices. We start with derivation of the interaction between the JV lattice and deformed PV stack via the interlayer Josephson energy, $E_J = E_J \int d^2r \cos \phi_n$ where ϕ_n is the phase difference between the layers n and $n+1$. The static dense JV lattice is characterized by the phase difference, $\phi_n(y) = k_H(y - y_J) + \phi_n$ with $k_H = 2\pi B_x / \phi_0$ and y_J describing the JV lattice displacement. The deformed PV stack with the coordinates $u_n = (u_{n,x}; u_{n,y})$ generates the additional phase difference

$$\phi_p(r; u_{n+1}; u_n) = \arctan \frac{y - u_{n+1,y}}{x - u_{n+1,x}} - \arctan \frac{y - u_{n,y}}{x - u_{n,x}}$$

and modifies the Josephson energy. In addition to interactions mediated by interlayer Josephson coupling, PVs are also aligned by the magnetic interaction¹. Due to its long-range nature, this interaction can be well approximated by a simple parabolic potential (see, e.g., Ref. 20) with the magnetic-spring constant, $K_p = \frac{1}{2} \mu_0 L = 4 \times 10^{-2}$ where $L = \ln(r_w)$ and $r_w = h(u_{n+1} - u_n)^2 i^{1/2}$ is the typical wandering distance. Therefore in a homogeneous superconductor the total energy change per one layer due to PV stack deformation is given by the sum of the Josephson and magnetic energies

$$E = \frac{1}{N} \sum_n \left((1 - \phi_n) E_J C(u_{n+1}; u_n; y_J) + \frac{K_p}{2} u_n^2 \right); \quad (1)$$

where N is the total number of layers and the function $C(u_2; u_1; y_J)$ in the lowest order with respect to the Josephson coupling energy, E_J , is given by

$$C(u_2; u_1; y_J) = \int d^2r \cos[k_H(y - y_J) + \phi_p(r; u_2; u_1)] \\ = \frac{I(k_H u_{12})}{k_H^2} \cos[k_H(y - y_J) + \frac{u_{1,y} + u_{2,y}}{2}] \quad (2)$$

with $u_{12} = u_2 - u_1$ and

$$I(v) = \int dxdy \int_0^1 \frac{r^2 - v^2}{r^2 + v^2} \cos y \\ + \frac{v_x y - v_y x}{r^2 + v^2} \sin y \quad (3)$$

with $v = k_H |u_{12}|$. In the regime $k_H |u_{12}| \ll 1$, this dimensionless function can be computed analytically up to the third order with respect to the reduced variable v ,

$$I(v) \approx 2v_x + \frac{v^2}{2} - \frac{v_x}{4} \ln \frac{C_h}{v} - \frac{v_x^2 - v_y^2}{4} + \frac{v_x v_y^2}{8} \quad (4)$$

with $v^2 = v_x^2 + v_y^2$ and $C_h = 8 \exp(-\gamma) \approx 4.492$ ($\gamma = 0.5772$ is the Euler constant). The linear in v_x term in $I(v)$ gives the linear-displacement contribution to the Josephson energy, $(4 E_J N k_H) \sum_n (1 - \phi_n) u_{n,x} \cos[k_H y_J]$. This term describes forces acting on the straight PV stack from the alternating in-plane currents induced by the JV lattice, $j_y(y; n) = (1 - \phi_n) j_h \cos[k_H(y - y_J)]$, where $j_h = (2\pi h) j_J$, $h = 2 B_x / \phi_0$ is the reduced magnetic field and $j_J = (2\pi c / \phi_0) E_J$ is the Josephson current density. Due to this term the ground state corresponds to the alternating PV deformations along the direction of the in-plane field⁵, $u_{n,x} = (1 - \phi_n) u_a$ with $u_a = (s / c) j_h / K_p = 4 \times 10^{-2} [h / s \ln(r_w)]$, see Fig. 1. For such deformations, the quadratic term in the Josephson energy cancels out and does not influence the deformation amplitude. The assumed condition $k_H u_a < 1$ is satisfied if $\gamma > s$.

Lets consider now dynamic behavior. A transport current applied across the layers drives the JV lattice along the layers. We consider the lattice slowly moving with constant velocity through the PV stacks along the y axis, $y_J = vt$. Such motion generates the electric field, $E_z = B_x v = c$. The lattice velocity is assumed to be much smaller than the Swihart velocity so that the lattice preserves its static structure. The homogeneously moving JV lattice forces PVs to oscillate with the Josephson frequency, $u_x(n;t) = (1)^n u_a(t)$, with $u_a(t) = u_{a0} \cos(\omega_E t + \phi)$ and $\omega_E = k_H v$. For a PV stack located near $y = 0$, the alternating deformation, $u_a(t)$, is described by a simple oscillator equation

$$K_p u_a + K_p u_a = f_h \cos(\omega_E t); \quad (5)$$

where $f_h = (s_0 = c) j_h = 4 s E_J = h$ and K_p is the pancake viscosity coefficient. Solution of this equation is given by

$$u_a(t) = \text{Re} \frac{f_h \exp(i \omega_E t)}{K_p + i \omega_E} : \quad (6)$$

The frequency response of the stacks is determined by the relaxation frequency, $\omega_r = K_p = \omega_p$. The oscillation amplitude drops at $\omega_E > \omega_r$.

The average friction force per PV acting on the moving JV lattice is given by

$$F_y = \frac{dE}{dy_J} = \frac{E_J}{N k_H} \sum_n (1)^n I k_H (u_{n+1} - u_n) \sin \omega_E t k_H \frac{u_{n,y} + u_{n+1,y}}{2} \quad (7)$$

where $\langle \dots \rangle$ denotes time averaging. In the regime when only small alternating deformations in the x direction are present, this gives $F_y = 4 E_J h u_a(t) \sin(\omega_E t)$, and, using the solution (6), we obtain

$$F_y = 2 E_J f_h \frac{\omega_E K_p}{K_p^2 + \omega_E^2}; \quad (8)$$

The average velocity of the JV lattice is connected with the applied current, j_z , by the force-balance condition

$$j_z v + n_p F_y + (B_x = c) j_z = 0 \quad (9)$$

where j_z is the bare ux-flow friction coefficient of the JV lattice and $n_p = B_z = s_0$ is the concentration of PVs, and the third term is the driving force from the transport current. This corresponds to the following current-voltage dependence

$$j_z(E_z) = j_z E_z + j(E_z) \quad (10)$$

where $j_z = (c = B_x)^2 j_z$ is the bare ux-flow conductivity and

$$j(E_z) = \frac{\omega_p F_y}{B_x} = \frac{\omega_p E_z}{1 + (s E_z = V_r)^2} \quad (11)$$

is the current enhancement due to the PV-induced damping of JV motion, which we will call excess pancake-vortex current, with $\omega_p = \omega_p(B_z; B_x) = 2^2 n_p s^4 j_h^2 = K_p^2$ and $V_r = [s_0 = (2/c) K_p = \omega_p]$ is the voltage drop per junction corresponding to the relaxation frequency. The electric-field dependence of the conductivity $j(E_z) = E_z$ resembles a well-known Drude frequency dependence. Introducing the pancake ux-flow conductivity $(B_z) =$

$\omega_p^2 = (s_0 B_z)$, we can express the conductivity and voltage scales, ω_p and V_r , via experimentally-accessible parameters

$$\omega_p = 2 (B_z) \frac{B_z = B}{(h)^2}; \quad V_r = \frac{c_0}{8^{1/2} (B_z)}$$

with $B_0 L = (4^{-1/2})$. Note that ω_p scales with the field components as $\omega_p / B_z = B_x^2$.

The key feature of the excess PV current, $j(E_z)$, is that it depends nonmonotonically on the electric field. The maximum current due to the pancake vortices can be estimated as $j_{max} = j_z (B_z = B) = h^2$. As ω_p / B_z , the total I-V dependence (10) becomes nonmonotonic at sufficiently large B_z . In fixed-current experiments this leads to voltage jumps. Eq. (10) also determines the angular dependence of voltage at fixed current frequently measured experimentally. Introducing the tilt angle of field, $B_z = B_x \sin \theta$, we can rewrite Eqs. (10) and (11) in the form

$$j_z = h [1 + (s E_z = V_r)^2]^{-1} \frac{j_z j_z E_z}{\omega_p E_z} \quad (12)$$

with $\omega_p = 4 (B_z)^2 = [3 s^2 L]$. This equation explicitly determines the dependence $E_z(\theta)$ at fixed j_z . In particular, in the case $V_r = s j_z = j_z$, the maximum and minimum of the dependence $E_z(\theta)$ are given by

$$j_{max} = \frac{h (s j_z)^2}{8^{1/2} j_z V_r^2} \text{ at } E_z = j_z = 2 j_z$$

$$j_{min} = \frac{2 h s j_z}{V_r} \text{ at } E_z = V_r = s$$

At these angles the voltage will have jumps. As we see, in a simple model both angles are proportional to the in-plane field. The angular dependence of the electric field

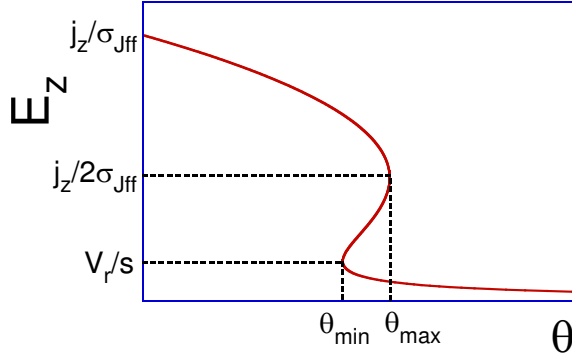


FIG. 2: The angular dependence of the electric field at fixed current following from Eq. (12) at $V_x = s j_z = J$. Voltage jumps are expected at the angles θ_{\max} and θ_{\min} .

following from Eq. (12) at $V_x = s j_z = J$ is illustrated in Fig. 2.

B. Friction force from fluctuating pancake-vortex stacks

In real experimental conditions the result may be strongly influenced by pinning and thermal fluctuations. Let us consider influence of thermal fluctuations. At a finite temperature, in addition to the regular zigzag deformations, the PV stack has random fluctuating displacement $u_{f;n} = (u_{f;x;n}; u_{f;y;n})$. These pancake fluctuations influence the damping of the JV lattice in several different ways. The most direct channel is that, due to random displacement in the y direction (perpendicular to the field), exact time periodicity of the force from the JV lattice acting on PV is perturbed. This leads to the Debye-Waller-like suppression of the pancake oscillation amplitude and reduction of the corresponding current enhancement. The PV displacements also modify the interaction force between PVs and JV lattice (in the low orders with respect to displacements this effect is described by Eq. (4)). Both above effects have the same order and become strong when the typical PV fluctuation becomes of the order of the JV lattice period. The pancake fluctuations also perturb phase distribution of the JV lattice leading to renormalization of its bare flux-flow resistivity. We will also estimate this effect.

We now analyze the fluctuation effects quantitatively. At finite temperature and for the homogeneously moving JV lattice, $y_J = vt$, the PV displacements obey the following equation

$$p u_n + K_p u_n + (1/E_J) \frac{\partial [C(u_{n+1}; u_n; vt) - C(u_n; u_{n-1}; vt)]}{\partial u_n} = f_{L,n}(t) \quad (13)$$

where the function $C(u_1; u_2; y_J)$ is defined by Eqs. (2) and (3) and $f_{L,n}(t)$ is the thermal Langevin force with

the correlation function

$$\langle f_{L,n}(t); f_{L,m}(t') \rangle = 2 p k_B T \delta_{nm} \delta(t - t') \quad (14)$$

This equation generalizes Eq. (5) for finite temperatures and large pancake displacements. Introducing the dimensionless variables for the time, $\tau = t/t_0$ and coordinate $x = x_H u$, we conclude that the overall behavior is determined by the two dimensionless parameters,

$$J = \frac{E_J}{K_p} = \frac{2}{(s)^2 L} \quad (14)$$

giving the relative strength of magnetic and Josephson couplings between PVs in different layers and the reduced temperature

$$T = \frac{k_H^2 k_B T}{K_p} = \frac{(2 s B_x)^2 (4)^2 k_B T}{2_0^2 L s^2_0} \quad (15)$$

This reduced temperature has a transparent physical meaning, at $T = 1$ the fluctuating pancake displacement becomes of the order of the JV lattice period. We can see that the relative strength of fluctuations rapidly increases with increasing in-plane field.

We numerically solved the dynamic Langevin equations for the pancake displacements u_n (13) with numerically computed dependence $I(v)$ from Eq. (3), and used obtained solution to compute the average friction force (7). Figure 3a shows the Josephson-frequency dependences of the friction force F_y for different reduced temperatures for typical value of the parameter J , $J = 0.1$. We can see that the main effect of fluctuations is suppression of the maximum of the $F_y(\omega)$ dependence corresponding to the maximum of $j(E_z)$. To quantify this suppression, we show in Fig. 3b temperature dependences of the maximum friction force for two values of the parameter J , 0.1 and 0.2. The maximum force decreases by factor of 2 at $T = 0.5$ –0.7. The maximum only slightly shifts to higher frequencies with increasing temperature. Also, at high temperatures the force decays slower than $1/\omega$ at large frequencies.

C. Reduction of the regular flux-flow conductivity by pancake-vortex fluctuations

Pancake fluctuations also perturb regular phase distribution in the moving JV lattice leading to modification of the regular flux-flow conductivity. This gives an additional channel of PV influence on the JV mobility. In this section we estimate this effect quantitatively. Dynamic behavior of the JV lattice in layered superconductors is described by the coupled reduced equations for the interlayer phase differences ϕ_n and reduced fields h_n , see, e.g., Ref. 21

$$\frac{\partial^2 \phi_n}{\partial t^2} + c \frac{\partial \phi_n}{\partial t} + \sin \phi_n + \frac{\partial h_{y,n}}{\partial x} - \frac{\partial h_{x,n}}{\partial y} = 0 \quad (16a)$$

$$r_n^2 \frac{1}{L^2} h_{x,n} + \frac{\partial \phi_n}{\partial y} + a b \frac{\partial \phi_n}{\partial t} - \frac{\partial \phi_n}{\partial y} \frac{h_{x,n}}{L^2} = 0 \quad (16b)$$

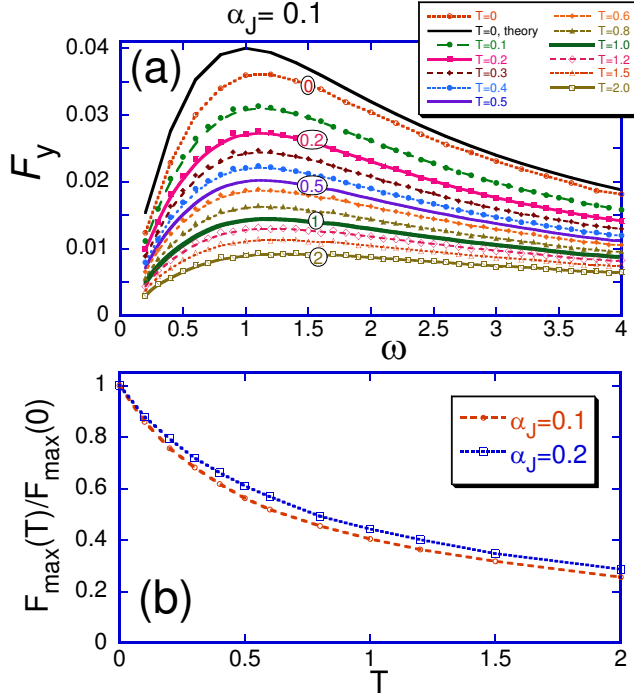


FIG. 3: (a) Evolution of the friction force vs Josephson frequency dependence with increasing reduced temperature (15) for $\alpha_J = 0.1$. In this plot F_y is the friction force induced by one fluctuating PV stack on JV lattice defined by Eq. (7) in units of $K_p = k_H$. The frequency unit is ω_r . The curves are calculated using pancake displacements obtained by direct numerical simulation of the Langevin dynamic equations (13). The upper solid line represents the analytical result (8) valid at $T = 0$ and $\alpha_J = 1$. (b) The temperature dependence of the maximum friction force for two values of the parameter α_J , 0.1 and 0.2.

In these equations the units of space and time are given by the Josephson length, λ_J , and the inverse plasma frequency, $1/\omega_p$, and α_{ab} are the dissipation parameters related to the quasiparticle conductivities, and $l = \alpha_{ab} s$. For the moving triangular lattice the phase differences can be represented as

$$\phi_n(\mathbf{r}; t) = \phi_E t - k_H y + \phi_n + \phi_{v,n}(\mathbf{r}; t) + \phi_n(\mathbf{r}; t)$$

where $\phi_{v,n}(\mathbf{r}; t) = \sum_j \phi_p(\mathbf{r} - \mathbf{R}_j; u_{n+1,j}(t); u_{n,j}(t))$ is the phase perturbation induced by PV displacements, $u_{n,j}(t)$, of the stack located at \mathbf{R}_j , $\phi_n(\mathbf{r}; t)$ is the correction due to the Josephson coupling. Solving Eqs. (16) by Fourier transform in the first order with respect to $\sin \phi_n$, we obtain

$$(k; q; !) = \frac{[\sin (!_E t - k_H y + \phi_n + \phi_{v,n}(\mathbf{r}; t))]_{k;!}}{(k; q; !)} \quad (17)$$

$$\text{with } (k; q; !) = !^2 i_c ! \frac{k^2 (1 + i_{ab} !)}{2(1 - \cos q) + (1 + i_{ab} !) = !^2};$$

where $[\cdot]_{k;!}$ notates Fourier transformation with respect to coordinate and time. To obtain I-V characteristic we have to evaluate the average reduced Josephson current $i_J = \langle \sin \phi_n(\mathbf{r}; t) \rangle$, which in the first order with respect to $\phi_n(\mathbf{r}; t)$ is given by

$$i_J = \langle \cos (!_E t - k_H y + \phi_n + \phi_{v,n}(\mathbf{r}; t)) \phi_n(\mathbf{r}; t) \rangle$$

Note that the PV excess current derived in the previous sections also can be obtained using this approach if we add to $\phi_n(\mathbf{r}; t)$ the dynamic phase perturbation due to the oscillating PVs.

Using result (17), we derive

$$i_J = \sum_{k,q;!} S(k; q; !) i_{J0}(k_H - k; q; !) \quad (18)$$

where $S(k; q; !)$ is the Fourier transform of the phase correlation function

$$S_n(\mathbf{r} - \mathbf{r}^0; t) = \langle \exp [i(\phi_{v,n}(\mathbf{r}; t) - \phi_{v,n}(\mathbf{r}^0; 0))] \rangle = \frac{1}{\exp(-(\phi_{v,n}(\mathbf{r}; t) - \phi_{v,n}(\mathbf{r}^0; 0))^2/2)}$$

and

$$i_{J0}(k; q; !) = \frac{1}{2} \text{Im} \frac{1}{(k; q; !)}$$

In particular, without PV fluctuations $S(k; q; !) = \langle \phi(\mathbf{k}) \phi(\mathbf{q}) \rangle$ and the average Josephson current is simply given by $i_{J0}(k_H; 0; !)$ giving at small $!_E$ the bare JV flux-flow resistivity (see Ref[21]).

Let us evaluate the phase correlation function $S_n(\mathbf{r}; t)$. Neglecting correlations between displacements in different stacks, we obtain

$$S_n(\mathbf{r} - \mathbf{r}^0; t) = 1 - \frac{B_z}{0} \int_0^Z dR (1 - \exp[-G(\mathbf{r} - \mathbf{R}; \mathbf{r}^0; R)]) \quad (19)$$

$$G(\mathbf{r}; \mathbf{r}^0) = \frac{1}{2} \int_0^D [\phi_p(\mathbf{r}; u_{n+1}(t); u_n(t)) - \phi_p(\mathbf{r}^0; u_1(0); u_0(0))]^2$$

Using expansion of the PV phase difference at $\mathbf{r} = \mathbf{r}_n$ with $w_n = u_{n+1} - u_n$, $\phi_p(\mathbf{r}; u_{n+1}; u_n) = [\mathbf{r} - \mathbf{w}_n]_z^2$, we can see that the integral over R logarithmically diverges at large R . Cutting off this divergency at $R = R_c$, we obtain with logarithmic accuracy the following result

$$S_n(\mathbf{r}; t) = 1 - \eta_w \frac{r_w^2}{r_w} \ln \frac{R_c}{r_w} = \langle w_n(t) w_0(0) \rangle \ln \frac{R_c}{r_w} \quad (20)$$

with $r_w^2 = w_n^2$. From Eqs. (18) and (20) we can conclude that the PV fluctuations reduce the regular contribution to the Josephson current and the relative reduction can be estimated as $j = j_0 \frac{r_w^2}{R_c} \ln(R_c/r_w)$. This correction roughly corresponds to suppression of the Josephson coupling in the area r_w^2 around the PV stack. At small velocities this reduction is typically much

smaller than the current increase due to pancake oscillations. However, as the PV excess current decays with increasing velocity, the regular contribution may become dominating at high velocities. The relative contribution of the regular term also increases with increasing temperature.

D. Role of columnar defects

Columnar defects produced by heavy-ion irradiation are known to be the most efficient pinners of PVs, see Ref. 22. Moreover, they effectively suppress fluctuation and align the PV stacks²³. Experimentally, this alignment leads to significant increase of the Josephson Plasma Resonance frequency²⁴. Therefore we can expect that the columnar defects will strongly suppress the PV-induced damping of JVs. Naively, one may think that effect of the columnar defects can be described by a simple enhancement of the effective spring constant in the confining parabolic potential. However, a more accurate analysis below shows that this is incorrect description. A columnar defect produces a very strong local potential for PVs, which is poorly described by the parabolic approximation. Due to a discrete nature of the PV stack, its statistical distribution around the columnar defect consists of two parts²³: a sharp peak centered at the defect corresponding to PV located inside the column and a very wide envelope function corresponding to PV located outside the column. In such situation, we can expect that PVs confined inside the column do not contribute to JV damping while PVs outside the column give almost the same contribution as free PVs. This means that the columnar defect simply reduce the excess current by the probability factor to find PV outside the columnar defect, P_{out} , as $j! P_{out}^j$. To estimate this probability, we consider a fluctuating pancake vortex near the columnar defect, which we model as an insulating disk with radius b . The ratio of probability to find the PV outside the column, P_{out} , to probability to find PV inside the column, P_{in} , can be evaluated as

$$\frac{P_{out}}{P_{in}} = \frac{\int_0^{\infty} \frac{d^2r}{s_0} \exp \left(-\frac{v_v(r)}{T} \right)}{1} \quad (21)$$

where $v_v(r)$ is the PV energy, measured with respect to the ground state corresponding to the PV located in the column center,

$$v_v(r) = U_p + s_0 \ln \left(1 + \frac{b^2}{r^2} \right) + K_p r^2 = 2;$$

with $s_0 = (c_0/4)^2$. The first term, $U_p = s_0 \ln(b=)$ is the pinning energy for $b > \lambda$, the second term is the interaction energy with columnar defect, and the third term is the magnetic coupling energy, s_0 is elemental area which can be evaluated by analyzing the Gaussian fluctuation of the order parameter in the vicinity of vortex core²⁵,

$$s_0 = \frac{C_s 2 \lambda^2 T}{\ln(\lambda/s_0)};$$

in which λ is the coherence length, $C_s = \frac{1}{4\pi} \frac{4\pi e^2 \hbar^2}{m^*} \frac{1}{\lambda^2}$ is the Ginzburg-Landau parameter, and $C_s \approx 1$. In contrast to consideration of Ref. 23, in the case of large in-plane field we can neglect Josephson interaction in between PVs in neighboring layers and take into account only magnetic coupling. The value of the integral (21) is determined by the competition between the two factors: the large energy cost $s_0 \ln(b=)$ for putting PV outside the column and large area of integration limited by the shallow magnetic-coupling parabolic potential. For estimate, we can neglect the long-distance tails $s_0 \ln(1 + \frac{b^2}{r^2})$ in the pinning potential. In this case we obtain the following estimate

$$\frac{P_{out}}{P_{in}} \approx \exp \left(-\frac{U_p}{T} - \frac{2T}{s_0 K_p} \right) \exp \left(\frac{s_0 \ln(b=)}{T} \right) \frac{2}{C_s}$$

Therefore, the probability to find PV outside the column can be estimated as

$$P_{out} = \frac{1}{1 + \exp[s_0 \ln(b=) = T] C_s} \quad (22)$$

Ratio P_{out}/P_{in} becomes of the order of 1 at the typical depinning temperature, T , which can be estimated as

$$T = \frac{s_0 \ln(b=)}{2 \ln(\lambda/s_0)} \quad (23)$$

The columnar defects strongly reduce the damping due to PVs at $T \approx T$ and this effect rapidly decreases at $T > T$. The value of this important temperature scale is most sensitive to the London penetration depth. For optimally doped BSCCO, assuming $\lambda(T) = 200 \text{ nm} = (1 - (T/T_c)^2)^{-1/2}$, $\lambda = 15 \text{ nm} = (1 - (T/T_c)^2)^{-1/2}$ with $T_c = 90 \text{ K}$, and $b = 7 \text{ nm}$, we estimate $T \approx 58 \text{ K}$. For weakly underdoped BSCCO, taking $\lambda(0) = 250 \text{ nm}$ and $T_c = 85 \text{ K}$, we obtain $T \approx 45 \text{ K}$.

III. EXPERIMENTAL RESULTS

Josephson flux-flow (JFF) measurements have been done on the two mesa structures fabricated from the BSCCO single-crystal whiskers using double-sided processing by the focused ion beam (FIB) technique²⁶, see Fig. 4. The mesas had geometrical sizes $L_a \times L_b \times L_c = 26 \text{ m} \times 5.8 \text{ m} \times (0.18-0.23) \text{ m}$ (mesa #1) and $20 \text{ m} \times 5 \text{ m} \times (0.5-0.6) \text{ m}$ (mesa #2). The mesa #1 was prepared out of the overdoped whisker grown in oxygen flow. The mesa #2 was prepared out of the underdoped whisker grown in a mixture of 10-20% of O_2 and 80-90% of Ar.

At fixed temperatures and fixed in-plane component of the magnetic field (H_{\parallel}) we measured the JV flux-flow resistance R at several fixed currents and the I-V characteristics as a function of the c-axis component of the field (H_{\perp}). The cryostats with two perpendicular coils have been used for these experiments, the main coil provided the parallel field component, H_{\parallel} , while another coil

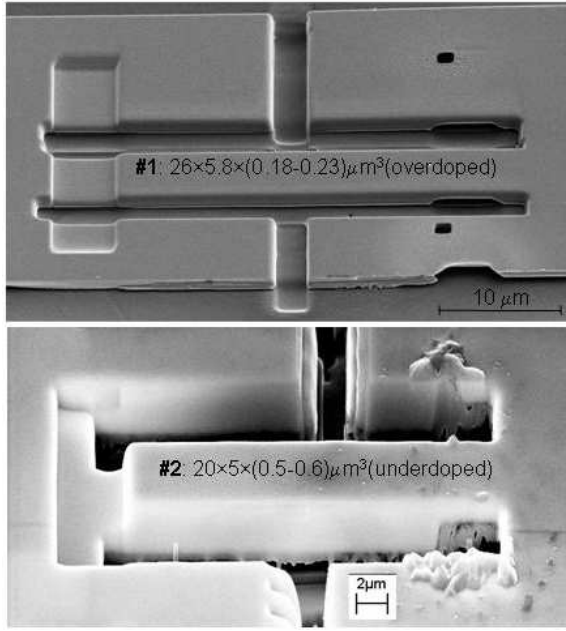


FIG. 4: Two mesa structures fabricated out of BSCCO whiskers for transport measurements.

induced the perpendicular component, H_z . The strictly parallel orientation has been found using sharp maximum of $R(H_z)$ dependence by sweeping H_z . We estimated an accuracy of field rotation in this way to be within 0.01. The experiments have been carried out at high temperatures above 40K to avoid flux trapping effects. As a separate part of the experiments, we studied the influence of columnar defects on the JFF with and without the perpendicular field component. The irradiation was made by Pb-ions with energy of 1 GeV at the GANIL accelerator (Caen, France). The defects were introduced into the mesa #2 along the c axis with concentration $3 \times 10^{10} \text{ cm}^{-2}$ corresponding to the matching field of about 60 Oe. For a comparison, the JFF characteristics have been measured in the mesa #2 first just before irradiation and then remeasured exactly at the same conditions within a week after irradiation.

Figure 5 (left panel) shows the dependence of the JFF voltage at fixed current on the c-axis magnetic field, H_z , for the mesa #1. We can see that the JFF voltage is highly sensitive to a small component of H_z resulting in large negative JFF magnetoresistance $R_{JFF}(H_z) = U(H_z)/I$. At the fixed current (0.2 mA) and fixed in-plane field (1 tesla) the JFF resistance first decreases linearly with H_z and then drops down sharply to the low-resistance state. To understand the mechanism of this drop, we show in the right panel of Fig. 5 a series of I-V dependences traced at the different fixed H_z values marked in the left plot. We can see from this plot, that the voltage drop to the low-resistance state originates from a nonmonotonic character of the I-V dependence which appears at high enough H_z . The excess current,

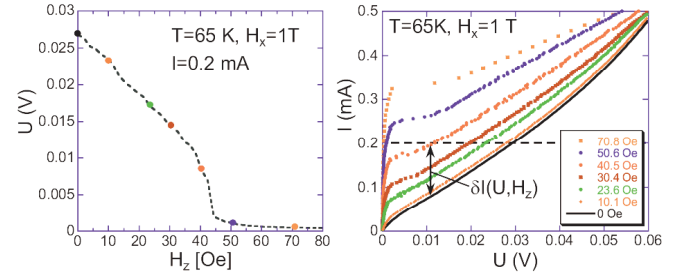


FIG. 5: Left plot shows H_z dependence of the z-axis voltage at fixed current $I = 0.2 \text{ mA}$ and in-plane field $H_x = 1 \text{ T}$ for the mesa #1. The right plot shows the current-voltage (I-V) dependences at several fixed H_z values marked in the left plot. The horizontal dashed line marks the current value in the left plot. One can see that the I-V dependence acquires a jump around $H_z \approx 500 \text{ e}$, which is coming from the nonmonotonic contribution, $I(U; H_z)$, from the pancake vortices. As a consequence, the H_z (or angular) dependence of voltage at fixed current in the left side also has a jump.

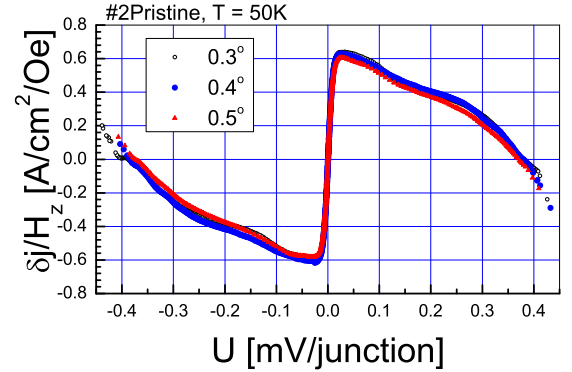


FIG. 6: Plots of the ratio $j=H_z$ vs voltage for $H_x = 1 \text{ T}$ and three tilt angles demonstrating that the excess pancake current is proportional to concentration of PVs.

$I(U; H_z) - I(U; H_z) - I(U; 0)$, in the I-V dependences is a direct consequence of an additional damping of the moving JV lattice induced by the PV stacks, as discussed in the theoretical sections above. Figure 6 shows plots of the ratios $j=H_z$ vs bias voltage U for the mesa #2 before irradiation at different tilt angles corresponding to different H_z . One can see nonmonotonic dependence $j(U)$, that first increases rapidly, reaches a maximum and then decreases slowly. Another remarkable feature is proportionality of j to H_z up to $H_z \approx 87 \text{ Oe}$ (0.5 tilt), which is seen from an almost ideal collapse of the $j=H_z$ curves at different tilt angles. Figure 7 shows the I-V dependences of the mesa #1 for two values of the in-plane field, $H_x = 1.04 \text{ T}$ and 2.08 T , and for very close values of c-axis field, $H_z \approx 40 \text{ Oe}$. We can see that for $H_x = 2.08 \text{ T}$ the amplitude of the excess current is more

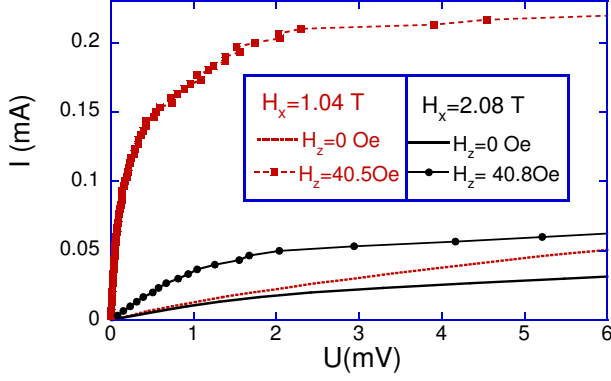


FIG. 7: The current-voltage dependences of the mesa # 1 for two values of the in-plane field, $H_x = 1.04\text{ T}$ and 2.08 T , and for very close values of c-axis field $H_z = 40.5$ and 40.8 Oe . For reference, the I-V dependences at $H_z = 0\text{ Oe}$ are also shown for both H_x . The amplitude of the excess PV current for $H_x = 2.08\text{ T}$ is more than four times smaller than for $H_x = 1.04\text{ T}$.

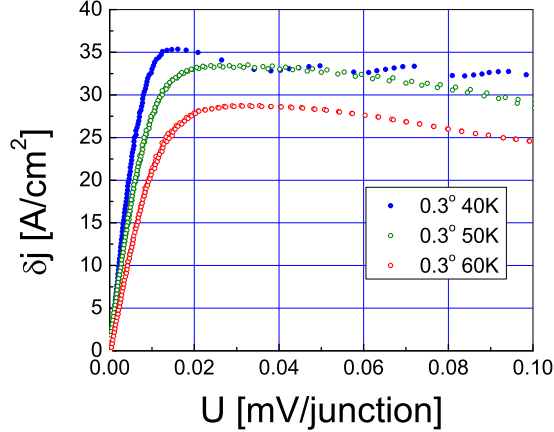


FIG. 8: Temperature evolution of the excess PV current density for the mesa # 2 at $H_x = 1\text{ T}$ and tilt angle 0.3° corresponding to $H_z = 52.4\text{ Oe}$. The voltage corresponding to maximum excess current decreases with decreasing temperature.

than four times smaller than for $H_x = 1.04\text{ T}$, which is consistent with the theoretical estimates. Figure 8 illustrates the temperature dependence of the excess current for the mesa # 2. We can see that at lower temperatures maximum in the excess current increases and moves to the lower voltages. We also note that for the overdoped mesa the excess PV current density is 4-5 times larger than for the underdoped one.

Figure 9 shows comparison of the PV-induced damping for the mesa # 2 before and after irradiation for three temperatures, 40 K, 50 K, and 60 K. It is interesting to

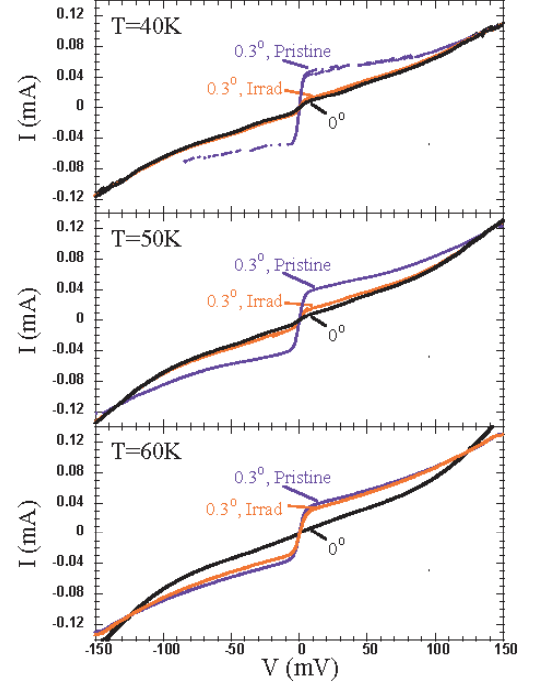


FIG. 9: Influence of heavy-ion irradiation on the pancake excess current. The current-voltage characteristics are shown for mesa # 2 before and after irradiation, for the magnetic field 1 T tilted at angle 0° and 0.3° (corresponding to $H_z = 52.4\text{ Oe}$). Irradiation dose corresponds to the matching field, $B = 60\text{ G}$. Irradiation does not influence motion of the JV lattice without PVs, at $H_z = 0$ but strongly reduces pancake effect at $T = 40\text{ K}$ and 50 K . This reduction is much weaker at 60 K .

note that the columnar defects induced by heavy-ion irradiation have negligible direct influence on dynamics of JV lattice (IVs at 0° tilt angles are not noticeably influenced by the irradiation). On the other hand, they strongly influence the PV-induced damping at low temperatures. We can see that at 40 K and 50 K pinning of the PV stacks by the columnar defects almost completely eliminates the PV extra damping. At 60 K this damping is restored most probably due to the thermal depinning of the PV stacks from the columns. This behavior is consistent with location of the thermal depinning temperature T evaluated in Sec. IID (for underdoped BSCCO we estimated $T \approx 45\text{ K}$).

IV. DISCUSSION

Strong dynamic interaction of the JVs with the PV stacks leads to a very high sensitivity of the JV transport to a very small concentration of the PV stacks which we observed experimentally. At a given driving force (or DC current) that interaction slows down the JV lattice and thus reduces the JFF voltage leading to the pro-

nounced negative JF F magnetoresistance with respect to the c-axis component of the magnetic field. On the other hand, at a given voltage the extra damping due to the PV stacks results in increase of the current. Theoretical description of these effects is based on calculation of the oscillating zigzag deformations of the PV stacks induced by the moving JV lattice and the average friction force due to these deformations. Several features of the experimental PV excess current, such as its nonmonotonic dependence on voltage, its decrease with increasing temperature and the in-plane field, are in a good qualitative agreement with the theory. A strong suppression of the PV damping by columnar defects also provides confirmation for suggested mechanism. A detailed quantitative comparison between the experiment and theory requires an accurate knowledge of the microscopic parameters of superconductor, London penetration depth, λ_{ab} , anisotropy γ , and pancake flux-flow resistivity ρ_{eff} , as well as geometrical parameters of the mesas.

To estimate the key theoretical parameters ρ_p and V_r we need values of the magnetic spring constant K_p and the PV viscosity coefficient, η_p . The magnetic spring constant is mainly determined by the London penetration depth. For example, taking a value $\lambda = 300\text{nm}$ typical for overdoped BSCCO at $T = 65\text{K}$, we obtain $K_p = 65\text{N/m}^2$ and $B = 36\text{G}$. The value of the viscosity coefficient is more uncertain. To our knowledge no direct transport measurement of the PV flux-flow resistivity in BSCCO has been published. Microwave measurements of the flux-flow resistivity in single crystals (at 40.8 GHz)²⁷ and films (at 48 GHz)²⁸ show that $\rho_p / d = dB_z$ has strong temperature dependence and suggest a typical value for $T = 60\text{K}$, $\rho_p = 10^8 - 10^7 \text{ N s/m}^2$ corresponding to the slope $d = dB_z = 2-20 \text{ cm/tesla}$. This gives the following estimate for the flux-flow conductivity at $B_z = B$, $(B)^2 \propto [Q \text{ cm}]^1$. These data suggest that the maximum PV effect is expected at very small voltage, $V_r = 0.1-1 \text{ V}$. Experimentally, the maximum excess current is observed at significantly higher voltages, $V_r = 15-30 \text{ V}$ corresponding to relaxation frequencies 7-15 GHz. Also, the simple theory does not quite describe shapes of the experimental $j(U)$ dependences, at $U > V_r$ the excess current decreases slower than expected $1/U$ decay. On the other hand, we found that shapes of $j(U)$ dependences also somewhat differ for underdoped and overdoped mesas. These discrepancies can be explained if we (i) assume small-velocity value for the viscosity constant, $\rho_p = 2 \cdot 10^6 \text{ N s/m}^2$, which is significantly larger than the microwave measurements suggest, and (ii) assume that it decreases with increasing PV velocity. In the temperature and in-plane field region probed in experiment influence of thermal fluctuation PV's considered in Sec. II B is significant. For example, for the overdoped mesa at 65 K, we estimate $\gamma = 0.15-0.2$ and the reduced temperature given by Eq. (15) as $T = 0.2$ for $B_x = 1\text{T}$ and 0.8 for $B_x = 2\text{T}$. Shape deviations, at least partly, can be due to the PV thermal fluctuations. Our calculations show that the PV

fluctuations mainly reduce the amplitude of j and somewhat weaken the dependence $j(U)$ at large U but they do not shift much the maximum of the $j(U)$ dependence.

Another possible reason for disagreement with the simple theoretical picture is that at small velocities the JV lattice may move inhomogeneously, via thermally-activated jumps. This regime of motion is not considered by the theory at all and it may lead to an increase of apparent V_r . We expect that this inhomogeneous regime is more pronounced for smaller sample sizes in which averaging over PV locations is incomplete. Therefore, a systematic size dependence of the effect would help to understand mechanism of the low-voltage regime.

Note that, due to a very small value of V_r , without scrutinizing I-V shape, the low-voltage enhancement of damping can be easily misinterpreted as an enhancement of the critical current. In our experiments, a detailed study of the small-voltage region shows that the JV lattice slowly moves below the maximum current meaning that this maximum is due to the enhancement of damping. This, of course, does not exclude possibility that in other experimental conditions (e.g., at low temperatures) the main PV effect would be enhancement of the critical current.

An extreme sensitivity of the JV flux-flow voltage to a very small concentration of the PVs suggests a very attractive possibility to use small-size mesas for detection of penetration of individual PV stacks which will be seen as current or voltage jumps. The change of the total current due to the penetration event of a single PV stack, I_1 , is expected to be independent on the mesa size and is given by

$$I_1 = \frac{d j}{dB_z} \bigg|_0$$

Its maximum value, $I_{1\text{max}}$, is realized at $V = V_r$ and at low temperatures, where thermal fluctuation suppression is small, can be estimated as

$$I_{1\text{max}} = j \frac{4}{h^2 \ln(\epsilon_r \epsilon_w)} :$$

Taking $j = 500\text{A/cm}^2$, $\lambda = 300\text{nm}$, and $h = 2$, we estimate $I_{1\text{max}} = 0.5 \text{ A}$. On the other hand, for the underdoped mesa #2 at 50K from Fig. 6 we obtain $I_{1\text{max}} = 0.12 \text{ A}$ consistent with the above theoretical estimate. For the overdoped mesa $I_{1\text{max}}$ is 4-5 times larger. Such currents are detectable experimentally. We conclude that this technique can be practically used for detection of the individual PV stacks penetration.

V. ACKNOWLEDGEMENTS

We would like to thank A.M. Nikitina for providing the BSCCO single-crystal whiskers, A. Ryhd, G. Karapetrov, and M. Gaifullin for valuable technical assistance. AEK also would like to thank K. Kadowaki and Y. Kakeya

for useful discussions. Work in Argonne was supported by the U.S. DOE, Office of Science, under contract # W-31-109-ENG-38. AEK and YIL acknowledge support from the NATO Travel grant No. PST.CLG.979047. The

work in Ecole Polytechnique was partially performed in the frame of the CNRS-RAS Associated European Laboratory between CRTBT and IRE "Physical properties of coherent electronic states in condensed matter".

- ¹ K.B. Efetov, Zh. Eksp. Teor. Fiz. 76, 1781 (1979) [Sov. Phys. JETP 49, 905 (1979)]; A.I. Buzdin and D. Feinberg, J. Phys. (Paris) 51, 1971 (1990); S.N. Artemenko and A.N. Kuglov, Phys. Lett. A 143 485 (1990); J.R. Clem, Phys. Rev. B 43, 7837 (1991).
- ² L.N. Bulaevskii and J.R. Clem, Phys. Rev. B, 44, 10234 (1991).
- ³ L.N. Bulaevskii, M. Ledvij, and V.G. Kogan, Phys. Rev. B 46, 366 (1992).
- ⁴ A.E. Koshelev, Phys. Rev. Lett. 83, 187 (1999).
- ⁵ C.A. Bolle, P.L. Gammel, D.G. Grier, C.A. Murray, D. J. Bishop, D.B.M. Itzian and A. Kapitulnik, Phys. Rev. Lett. 66, 112 (1991).
- ⁶ T. Matsuda, O. Kamimura, H. Kasai, K. Harada, T. Yoshida, T. Akashi, A. Tonomura, Y. Nakayama, J. Shimoyama, K. Kishio, T. Hanaguri, and K. Kitazawa, Science, 294, 2136 (2001).
- ⁷ I.V. Grigorieva, J.W. Steeds, G. Balakrishnan, and D.M. Paul, Phys. Rev. B 51, 3765 (1995).
- ⁸ A. Grigorenko, S. Bending, T. Tamagai, S. Ooi, and M. Henini, Nature 414, 728 (2001).
- ⁹ V.K. Vlasov-Vlasov, A.E. Koshelev, U. Welp, G.W. Crabtree, and K. Kadowaki, Phys. Rev. B 66, 014523 (2002).
- ¹⁰ M. Tokunaga, M. Kobayashi, Y. Tokunaga, and T. Tamagai, Phys. Rev. B 66, 060507(R) (2002).
- ¹¹ S. Bending and M.J.W. Dodgson, J. Phys.: Condens. Matter 17, R955 (2005).
- ¹² J.U. Lee, J.E. Nordman, and G. Hohenwarter, Appl. Phys. Lett., 67, 1471 (1995); J.U. Lee, P. Gupatasama, D. Hombaker, A. El-Kortas, D. Hinks, and K.E. Gray Appl. Phys. Lett., 71, 1412 (1997).
- ¹³ G. Hecht scher, R. Kleiner, A.V. Ustinov, and P. Muller, Phys. Rev. Lett. 79, 1365 (1997); G. Hecht scher, R. Kleiner, K. Schlenga, W. W alkenhorst, P. Muller, and H. L. Johnson, Phys. Rev. B, 55, 14638 (1997).
- ¹⁴ Yu.I. Latyshev, P. Monceau, and V.N. Pavlenko, Physica C 282-287, 387 (1997); Physica C 293, 174 (1997); Yu. I. Latyshev, M.B. Gaifullin, T. Yamashita, M. Machida, and Y. Matsuda, Phys. Rev. Lett., 87, 247007 (2001).
- ¹⁵ L.N. Bulaevskii, M. Maley, H. Safar, and D. Dominguez, Phys. Rev. B 53, 6634 (1996).
- ¹⁶ Yu. Latyshev and A. Volkov, Physica C, 182, 47 (1991)
- ¹⁷ H. Enriquez, N. Bonemps, P. Fournier, A. Kapitulnik, A. Maignan, and A. Ruyter Phys. Rev. B, 53, R14757 (1996)
- ¹⁸ G. Hecht scher, R. Kleiner, K. Schlenga, W. W alkenhorst, P. Muller, and H. L. Johnson Phys. Rev. B 55, 14638 (1997).
- ¹⁹ A.E. Koshelev, Phys. Rev. B 68, 094520 (2003).
- ²⁰ M.J.W. Dodgson, A.E. Koshelev, V.B. Geshkenbein, and G. Blatter, Phys. Rev. Lett. 84, 2698 (2000).
- ²¹ A.E. Koshelev and I. A. Ranson, Phys. Rev. B 64, 174508 (2001).
- ²² L. Civalé, A.D. Marwick, T.K. Worthington, M.A. Kirk, J.R. Thompson, L. K. Kusun-Eibaum, Y. Sun, J.R. Clem, and F. Holtzberg, Phys. Rev. Lett., 67(5), 648 (1991); M. Konczykowski, F. Rullier-Albenque, E. R. Yacoby, A. Shaulov, Y. Yeshurun, and P. Lejay, Phys. Rev. B, 44, 7167 (1991); W. Gerhauser, G. Ries, H.W. Neumüller, W. Schmidt, O. Eibl, G. Saemann-Ischenko, and S. K laum unzer, Phys. Rev. Lett., 68, 879 (1992); L. Civalé, Supercond. Sci. Technol. 10 A11 (1997); C.J. van der Beek, M. Konczykowski, R. J. Drost, P.H. Kes, N. Chikumoto, and S. Bouard, Phys. Rev. B 61, 4259 (2000).
- ²³ A.E. Koshelev, P. Le Doussal, and V.M. Vinokur, Phys. Rev. B 53 R8855 (1996).
- ²⁴ M. Sato, T. Shibauchi, S. Ooi, T. Tamagai, and M. Konczykowski, Phys. Rev. Lett. 79, 3759 (1997); M. Kosugi, Y. Matsuda, M.B. Gaifullin, L.N. Bulaevskii, N. Chikumoto, M. Konczykowski, J. Shimoyama, K. Kishio, K. Hirata, and K. Kumagai, Phys. Rev. Lett. 79, 3763 (1997)
- ²⁵ A.E. Koshelev, Phys. Rev. 50 506 (1994).
- ²⁶ Yu. I. Latyshev, S.-J. Kim, and T. Yamashita, IEEE Trans. on Appl. Supercond., 9, 4312 (1999).
- ²⁷ T. Hanaguri, T. Tsuboi, Y. Tsuchiya, Ken-ichi Sasaki, and A. M aeda, Phys. Rev. Lett. 82, 1273 (1999).
- ²⁸ E. Silva, R. Fastampa, M. G iura, R. M aroon, D. Neri, and S. Sarti, Supercond. Sci. Technol., 13 1186 (2000).